PROCEEDINGS OF SCIENCE

Dirac Eigenvalue Spectrum at Finite Temperature Using Domain Wall Fermions

Zhongjie Lin* **(HotQCD Collaboration)**
Department of Physics, Columbia University, New York, NY 10027, USA
E-mail: jasper@phys.columbia.edu

We present a study of the Dirac eigenvalue spectrum near the region of the QCD phase transition. This study makes use of a sequence of ensembles with temperatures from 150 MeV to 200 MeV generated with $2+1$ flavors of dynamical domain wall fermions (DWF) and the dislocation suppressing determinant ratio (DSDR) action on a $16^3 \times 8$ lattice with an extent of 32 or 48 in the fifth dimension. All the simulations lie on a line of constant physics with 200 MeV pions. The DWF Dirac operator is normalized using the methods of Giusti and Luscher combined with those of Rome-Southampton collaboration, allowing a direct evaluation of the Banks-Casher relation. The relation between the resulting temperature-dependent Dirac eigenvalue spectrum and the possible restoration of $U(1)_A$ symmetry with increasing temperature is discussed.

XXIX International Symposium on Lattice Field Theory
July 10-16, 2011
Squaw Valley, Lake Tahoe, California

*Speaker.

PoS(Lattice 2011)204

1. Introduction

The chiral phase transition is one of the most fundamental features of QCD. Lattice field theory has been applied successfully to the study of this interesting phenomena and the associated symmetries. While traditional lattice techniques measure the chiral observables in a straightforward manner, examining the low-lying part of the eigenvalue spectrum of the Dirac operator can provide unique insights into various aspects of the symmetry breaking or restoration that accompany the phase transition.

For instance, the chiral condensate, the chiral order parameter for the transition, can be expressed in terms of the eigenmode density via the following relation:

$$-\langle\bar{\psi}_q\psi_q\rangle = \int \mathrm{d}\lambda\, \rho(\lambda)\frac{2m_q}{m_q^2+\lambda^2}\,, \qquad q = l,s, \tag{1.1}$$

where $\rho(\lambda)$ is the spectral density of the Dirac operator and m_q is the quark mass. When the chiral and infinite-volume limits are taken, one will obtain the well-known Banks-Casher relation [1],

$$\lim_{m_l\to 0}\lim_{V\to\infty} -\langle\bar{\psi}_l\psi_l\rangle = \pi \lim_{\lambda\to 0}\lim_{m_l\to 0}\lim_{V\to\infty}\rho(\lambda). \tag{1.2}$$

In lattice calculation one may also examine the subtracted chiral condensate defined as,

$$\Delta_{l,s} = \langle\bar{\psi}_l\psi_l\rangle - \frac{m_l}{m_s}\langle\bar{\psi}_s\psi_s\rangle\,. \tag{1.3}$$

The subraction removes the ultraviolet divergent piece of the chiral condensate which is linear in quark mass.

The Dirac eigenvalue spectrum can be utilized to study the anomalous $U(1)_A$ symmetry as well. A similar order parameter $\Delta_{\pi-\delta}$, which is the difference between the pseudoscalar and scalar susceptibilities, can also be related to the eigenvalue spectrum,

$$\Delta_{\pi-\delta} \equiv \frac{\chi_\pi - \chi_\delta}{T^2} = \frac{1}{T^2}\int \mathrm{d}\lambda\ \rho(\lambda)\frac{4m_l^2}{\left(m_l^2+\lambda^2\right)^2}\,. \tag{1.4}$$

The expression above suggests that if there is a finite region above zero where the eigenvalue density vanishes (a gap), the $U(1)_A$ symmetry might be effectively restored.

With chiral symmetry under good control, domain wall fermions (DWF) [2, 3] are an optimum tool for the exploration of the phase transition region. The residual chiral symmetry breaking (present in the DWF formalism for finite fifth-dimensional extent L_s) is reflected in an additive correction to the bare quark mass (m_{res}), which can be further suppressed by the adoption of the dislocation suppression determinant ratio (DSDR) action [4, 5, 6]. Despite some unphysical, massive degrees of freedom from the extra fifth dimension, the low modes of the DWF Dirac operator should resemble an ordinary four-dimensional discretized version of QCD. Moreover, within the DWF formalism, the $U(1)_A$ symmetry is only broken by axial anomaly, rather than spoiled by lattice artifacts as with staggered fermions.

2. Implementation Details

We have collected eight ensembles near the phase transition region with $2+1$ flavors of fermions. All the simulations have a $16^3 \times 8$ space-time volume and a fifth dimension of $L_S = 32$ or 48 and they all lie on a line of constant physics with $m_\pi \approx 200$MeV and kaon mass almost physical [7]. Table 1 gives the basic parameters of these finite-temperature ensembles. The $N_{\rm cfg}$ column lists the number of configurations for which the eigenvalues are calculated. Figure 1 shows the disconnected susceptibilities of various temperatures and indicates a critical temperature around 160 MeV.

T (MeV)	β	L_s	$m_{\rm res}a$	$m_l a$	$m_s a$	$\frac{\langle\bar\psi\psi\rangle_l}{T^3}$	$\frac{\Delta\bar\psi\psi}{T^3}$	$\frac{\chi_{l,\rm disc}}{T^2}$	$N_{\rm cfg}$	$Z^{(\pi)}_{\rm tw\to m_f}$
140	1.633	48	0.00612	-0.00136	0.0519	6.26(12)	7.74(12)	36(3)	-	-
150	1.671	48	0.00296	0.00173	0.0500	6.32(29)	6.10(29)	41(2)	340	1.980(7)
150	1.671	32	0.00648	-0.00189	0.0464	8.39(10)	7.06(10)	44(3)	340	1.905(6)
160	1.707	32	0.00377	0.000551	0.0449	5.25(17)	4.83(17)	43(4)	408	1.725(8)
170	1.740	32	0.00209	0.00175	0.0427	4.03(18)	2.78(18)	35(5)	239	1.631(11)
180	1.771	32	0.00132	0.00232	0.0403	3.16(15)	1.56(15)	25(4)	246	1.476(4)
190	1.801	32	0.00076	0.00258	0.0379	2.44(9)	0.71(9)	11(4)	374	1.439(3)
200	1.829	32	0.00046	0.00265	0.0357	2.19(8)	0.47(8)	10(3)	710	1.365(3)
0	1.750	32	0.00188	0.00300	0.0370	-	-	-	252	1.5685(5)

Table 1: Summary of ensembles and the renormalization factors for the eigenvalue density.

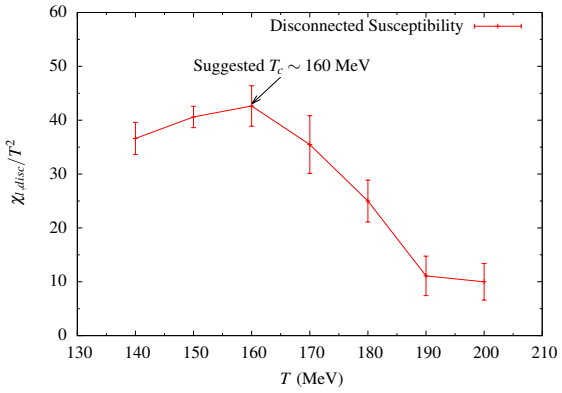

Figure 1: Disconnected susceptibilites.

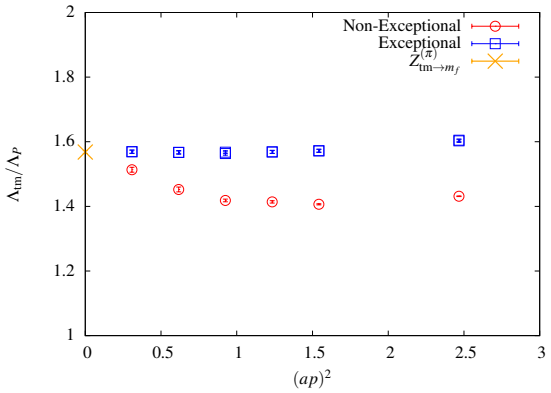

Figure 2: Renormalization factors for the $\beta = 1.750$, $16^3 \times 16$ ensemble.

For comparison, results from a zero-temperature ensemble with a volume of $16^3 \times 16$ are presented as well. In order to keep $m_\pi = 200$ MeV as the temperature and β decreases and $m_{\rm res}$ grows we must either increase L_s above 32 or use a negative input quark mass. As the second and third lines of Table 1 show, this first use of a negative DWF input quark mass was successful, resulting in no exceptional configurations and giving a consistent result for $\chi_{l,\rm disc}$.

We used the Kalkreuter-Simma [8] method to calculate the lowest $N_{\rm eig} = 100$ eigenvalues of the Hermitian version of the Dirac operator $D_H \equiv R^5\gamma^5 D_{\rm DWF}$, where R^5 is the reflection operator in the fifth dimension. Note the eigenvalues measured here include the mass term and are denoted by Λ, to be distinguished from those in the equations 1.1, 1.2 and 1.4.

3. Eigenvalue spectrum and its renormalization

Renormalization must be applied to the eigenvalue spectrum of the DWF operator D_H before any sensible comparison can be made with either the input DWF quark mass m_f or the eigenvalue densities from other four-dimensional fermion formalisms (*e.g.* Wilson fermions). The method we have adopted is a generalization to DWF of that proposed by Giusti and Luscher [9], which introduces into the Lagrangian a twisted mass term,

$$\mathscr{L}_{\rm tm}(x) = \sum_{j=1}^{k} \overline{q}^j(x) \left(\gamma^\nu D_\nu + m + i\mu\gamma^5\tau^3\right) q^j(x). \tag{3.1}$$

Then Green's functions such as the six-point correlator of the charged pseudoscalar density operator $P^{\pm}_{ll'} = \overline{q}^l(x)\gamma^5\tau^{\pm}q^{l'}(x)$ can be expressed in terms of the eigenvalue density,

$$\begin{aligned}
\sigma_3(\mu) &= -\sum_{x_i} \left\langle P^+_{1,2}(x_1)P^-_{2,3}(x_2)P^+_{3,4}(x_3)P^-_{4,5}(x_4)P^+_{5,6}(x_5)P^-_{6,1}(x_6)\right\rangle &(3.2)\\
&= \left\langle \mathrm{Tr}\left\{ \frac{1}{\left((\gamma^5 D)^2+\mu^2\right)^3}\right\}\right\rangle &(3.3)\\
&= \int_{-\infty}^{\infty} \mathrm{d}\Lambda\rho(\Lambda)(\Lambda^2+\mu^2)^{-3}, &(3.4)
\end{aligned}$$

in the notation of Giusti and Luscher [9]. The charged pseudoscalar density is well defined in the continuum limit in a variety of regularization schemes which are related by multiplicative renormalization factors. Equation 3.4 implies the same rules also will work for the eigenvalue density *e.g.*:

$$P'^i_{ll'} = \frac{1}{Z_{m\to m'}} P^i_{ll'} \quad \Longrightarrow \quad \rho'(\Lambda') = Z^{-1}_{m\to m'}\rho\left(\frac{\Lambda'}{Z_{m\to m'}}\right) \tag{3.5}$$

where $Z_{m\to m'}$ is the renormalization factor for the mass term treated symmetrically with $P^{\pm}_{ll'}$.

With such inspiration, we can invent a five-dimensional analogue of the twisted-mass term $P^{\mathrm{DWF},i}_{ll'}(x) = \sum_{s=0}^{L_s-1}\overline{\Psi}_l(x,s)\gamma^5\tau^i\Psi_{l'}(x,L_s-1-s)$ and relate it to the usual pseudoscalar density,

$$\overline{\psi}(x)\gamma^5\psi(x) \approx \frac{1}{Z_{\mathrm{tw}\to m_f}} \sum_{s=0}^{L_s-1} \overline{\Psi}(x,s)\gamma^5\Psi(x,L_s-1-s), \tag{3.6}$$

where $\psi(x)$ is the four-dimensional operator while $\Psi(x,s)$ is the five-dimensional field. [1] This renormalization factor $Z_{\mathrm{tw}\to m_f}$ connects the five-dimensional eigenvalue density to a more conventional density normalized in a fashion consistent with the usual bare quark mass m_f:

$$\rho^{m_f}(\Lambda^{m_f}) = Z^{-1}_{\mathrm{tw}\to m_f}\rho(\Lambda^{(5d)}), \qquad \Lambda^{m_f} = Z_{\mathrm{tw}\to m_f}\Lambda^{(5d)}. \tag{3.7}$$

Because of the equivalence of the two operators at long distance expressed by equation 3.6, the renormalization factor can be obtained from the ratio of the two Green's functions:

$$Z^{(\pi)}_{\mathrm{tw}\to m_f} = \frac{\left\langle \sum_{\vec{x}} \overline{\Psi}(\vec{x},t)R_5\gamma^5\tau^i\Psi(\vec{x},t)O^i_\pi(0)\right\rangle}{\left\langle \sum_{\vec{x}} \overline{\psi}(\vec{x},t)\gamma^5\tau^i\psi(\vec{x},t)O^i_\pi(0)\right\rangle}, \tag{3.8}$$

[1] The explicit sum over the fifth (s) dimension is suppressed later on for simplicity if no confusion is caused.

where τ_i's are the Pauli matrices in the flavor space. Results from a Coulomb gauge fixed wall source are presented in Table 1.

An alternative approach is to examine the off-shell, three-point Green's functions evaluated in Landau gauge. This is very similar to the Rome-Southampton non-perturbative renormalization (NPR) technique (RI/MOM) [10]. The renormalization factor is extracted from the ratio of amputated vertices for the five- and four-dimentional operators.

$$Z^{(\mathrm{MOM})}_{\mathrm{tw}\to m_f}(p_1,p_2) = \frac{\mathrm{Tr}\left\langle \sum_{x_1,x_2} e^{i(p_2x_2-p_1x_1)} \psi_l(x_2)\overline{\Psi}_l(0) R_5\gamma^5 \Psi_{l'}(0)\overline{\psi}_{l'}(x_1)\right\rangle}{\mathrm{Tr}\left\langle \sum_{x_1,x_2} e^{i(p_2x_2-p_1x_1)} \psi_l(x_2)\overline{\psi}_l(0)\gamma^5 \psi_{l'}(0)\overline{\psi}_{l'}(x_1)\right\rangle}. \tag{3.9}$$

To fully utilize the whole lattice, we use a series of fixed-momentum volume sources to calculate the propagators, which is defined as

$$\eta(x;p) = e^{ip\cdot x}\mathbb{I}_{4\times4}\otimes\mathbb{I}_{3\times3}\,. \tag{3.10}$$

We perform our calculation using both non-exceptional kinematics, where $p_1^2 = p_2^2 = (p_1-p_2)^2$, and exceptional kinematics, where $p_1 = p_2$. The results for the zero-temperature ensembles are presented in Table 1 and Figure 2.

Both Equation 3.8 and 3.9 should give consistent results independent of temporal separation t and of p_1 and p_2 respectively. Unfortunately, the NPR calculation is not feasible for the finite temperature ensembles due to large fluctuations. Therefore we only present the NPR results for the $16^3\times16$ emsemble in Figure 2. Figure 2 shows a discrepancy between the two kinematics which is positively related to the physical momenta. This contradicts our expectation but can be plausibly explained by appreciable finite lattice spacing errors $(ap)^2$ at large momentum. Because the quantity $Z^{(\pi)}_{\mathrm{tw}\to m_f}$ involves the smallest momenta, we use it to renormalize the spectrum.

Further renormalzation from the bare m_f scheme to the conventional, continuum $\overline{\mathrm{MS}}$ scheme can then be easily performed since this final step has already been studied in detail [11]. Technical details and updated results will be available in our upcoming paper [12].

Figure 3 displays the effects of the renormalization, which can be naively regarded as a rescaling of the axes. The orange vertical line denotes the smallest of the hundredth eigenvalue and the spectrum below that is supposed to be complete. The other vertical lines indicate the bare masses of the light and strange quarks. The horizontal lines are the chiral condensates divided by π, which should agree with the eigenvalue density at $\lambda = 0$ as predicted by Banks-Cahser relation 1.2. There are two significant features associated with the renormalization. First, the light quark mass now matches the likely zero-mode peak. Second, the Banks-Casher relation agrees better although it is still inaccurate at 30% level. We attribute the discrepancy to finite-volume and finite-mass effects. Thus, no definitive conclusion can be drawn before studies on a larger lattice and the chiral extrapolation are performed.

Figure 4 shows the renormalized eigenvalue spectra at various temperatures near the phase transition region. Although not in perfect agreement with the Banks-Casher relation, at lower temperatures such as 150 and 160 MeV the chiral condensates and the eigenvalue densities are different from zero, signaling spontaneous chiral symmetry breaking. Above 170 MeV, these two quantities both start to vanish as expected for temperatures above the transition. However, it remains uncertain whether the slope of the eigenvalue density vanishes before 190 and 200 MeV, where a

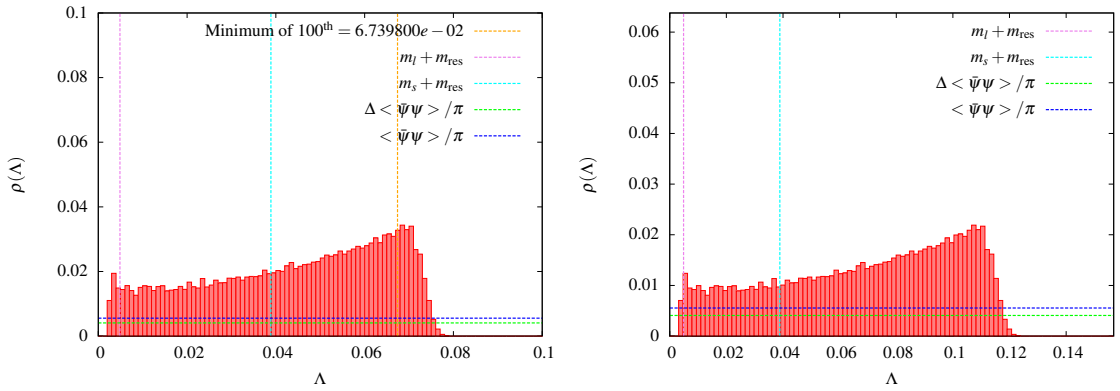

Figure 3: Dirac eigenvalue spectrum for the $\beta = 1.750$, $16^3 \times 16$, zero temperature ensemble. The density in the left-hand panel has not been renormalized while that on the right has been changed into the normalization scheme of the usual input DWF mass m_f. The left-most vertical line locates the total bare quark mass, $m_f + m_{\rm res}$ which matches well with the small peak seen in the renormalized, right-hand spectrum.

possible gap does begin to emerge, indicating an effective restoration of $U(1)_A$ symmetry. A small peak at the lower end at these temperatures suggests that the major contribution to $U(1)_A$ symmetry breaking may come from zero-modes, which are expected to go away as the volume increases. Therefore, we await a calculation on a larger lattice to confirm this conclusion.

4. Conclusions

With the chirally symmetric DWF framework, we are able to explore the chiral and $U(1)_A$ symmetries near the phase transition region. The successfully renormalized eigenvalue spectrum of the Dirac operator as well as the correlator measurements [13] suggest an effective restoration of the $U(1)_A$ symmetry at temperatures higher than T_c. We are looking forward to a similar simulation with larger volume to confirm our findings.

I very much appreciate the help and advice from members of HotQCD and my colleagues at Columbia University. This work was supported in part by U.S. DOE grant DE-FG02-92ER40699. The simulations were carried out on the BG/P machine at LLNL, the DOE- and RIKEN-funded QCDOC machines and NYBlue machine at BNL.

References

[1] T. Banks, and A. Casher, *Nucl.Phys.* **B169**, 103 (1980), revised Version.

[2] D. B. Kaplan, *Phys.Lett.* **B288**, 342–347 (1992), hep-lat/9206013.

[3] V. Furman, and Y. Shamir, *Nucl.Phys.* **B439**, 54–78 (1995), hep-lat/9405004.

[4] P. M. Vranas pp. 11–26 (1999), hep-lat/0001006.

[5] H. Fukaya, et al., *Phys.Rev.* **D74**, 094505 (2006), hep-lat/0607020.

[6] D. Renfrew, et al., *PoS* **LAT2008**, 048 (2008). arxiv:0902.2587.

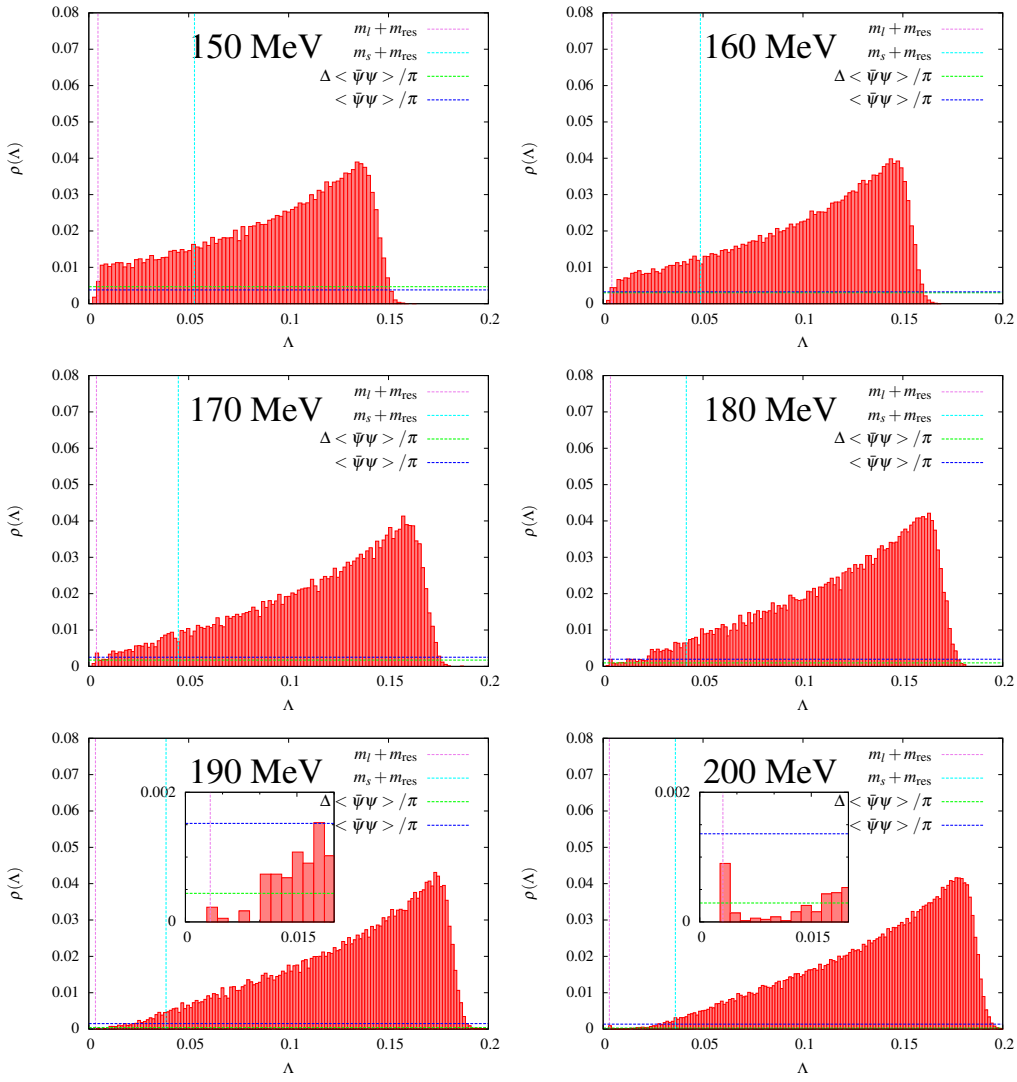

Figure 4: Dirac eigenvalue spectrum for the $T = 150 - 200$ MeV ensembles. Here the temperature is lowest in the upper left and largest in the lower right. The chiral symmetry breaking density of near zero eigenvalues disappears rapidly with increasing temperature and for the two highest temperature cases there appears to be a gap with very few eigenvalues just above zero. The magnified inset in these two cases show some near zero eigenvalues and a suggestive zero mode peak located at $\Lambda = m_f + m_{\rm res}$

[7] M. Cheng, *PoS* **LAT2011**, 186 (2011).

[8] T. Kalkreuter, and H. Simma, *Comput.Phys.Commun.* **93**, 33–47 (1996), hep-lat/9507023.

[9] L. Giusti, and M. Luscher, *JHEP* **0903**, 013 (2009), 0812.3638.

[10] G. Martinelli, et al., *Nucl.Phys.* **B445**, 81 (1995), hep-lat/9411010.

[11] Y. Aoki, et al., *Phys.Rev.* **D83**, 074508 (2011). 1011.0892

[12] M. Cheng, et al., *in preparation* (2011).

[13] P. Hegde, *PoS* **LAT2011**, 014 (2011).